Обзор ArXiv: astro-ph, 18-22 сентября 2017 года

От Сильченко О.К.

Astro-ph: 1709.04945

LoCuSS: The infall of X-ray groups onto massive clusters

C. P. Haines[1,2⋆], A. Finoguenov[3,4], G. P. Smith[5], A. Babul[6], E. Egami[7], P. Mazzotta[8], N. Okabe[9], M. J. Pereira[7], M. Bianconi[5], S. L. McGee[5], F. Ziparo[5], L. E. Campusano[2], C. Loyola[2]

[1] *INAF - Osservatorio Astronomico di Brera, via Brera 28, 20121 Milano, Italy*
[2] *Departamento de Astronomía, Universidad de Chile, Casilla 36-D, Correo Central, Santiago, Chile*
[3] *Max-Planck-Institut für extraterrestrische Physik, Giessenbachstrae, 85748 Garching, Germany*
[4] *Department of Physics, University of Helsinki, Gustaf Hällströmin katu 2a, FI-0014 Helsinki, Finland*
[5] *School of Physics and Astronomy, University of Birmingham, Edgbaston, Birmingham, B15, 2TT, UK*
[6] *Department of Physics and Astronomy, University of Victoria, 3800 Finnerty Road, Victoria, BC, V8P 1A1, Canada*
[7] *Steward Observatory, University of Arizona, 933 North Cherry Avenue, Tucson, AZ 85721, USA*
[8] *Dipartimento di Fisica, Università degli Studi di Roma 'Tor Vergata', via della Ricerca Scientifica 1, 00133 Roma, Italy*
[9] *Department of Physical Science, Hiroshima University, 1-3-1 Kagamiyama, Higashi-Hiroshima, Hiroshima 739-8526, Japan*

18 September 2017

ABSTRACT

Galaxy clusters are expected to form hierarchically in a ΛCDM universe, growing primarily through mergers with lower mass clusters and the continual accretion of group-mass halos. Galaxy clusters assemble late, doubling their masses since $z\sim0.5$, and so the outer regions of clusters should be replete with infalling group-mass systems. We present an *XMM-Newton* survey to search for X-ray groups in the infall regions of 23 massive galaxy clusters ($\langle M_{200}\rangle\sim10^{15}\,M_{\odot}$) at $z\sim0.2$, identifying 39 X-ray groups

В каждой площадке – и падающие на скопление группы (красные), и группы поля (синие)

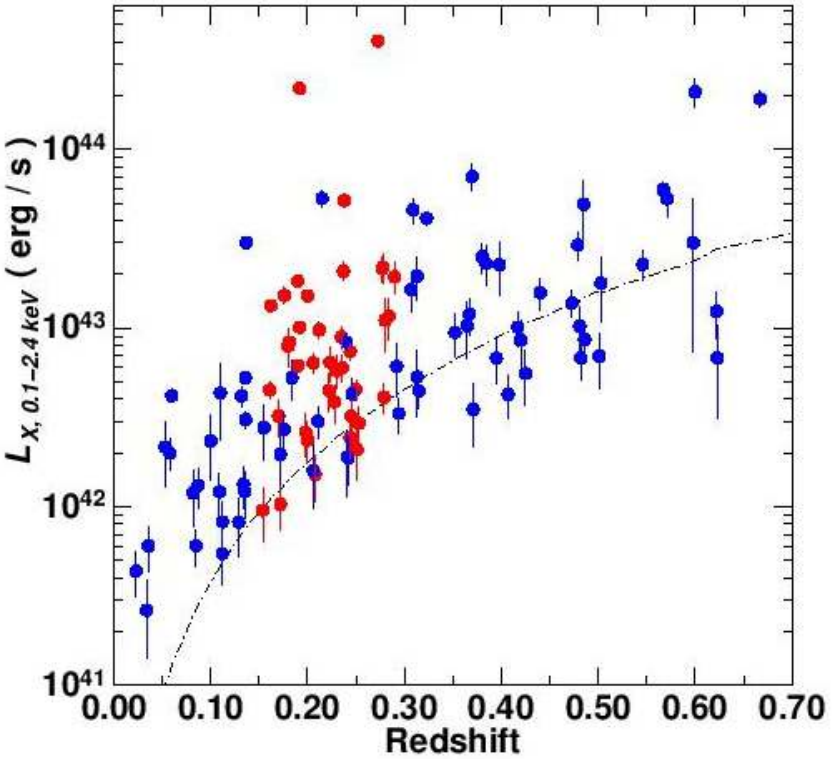

Figure 1. X-ray luminosity-redshift sampling of all the galaxy groups detected in the *XMM* images with a confirmed spectroscopic redshift. Those galaxy groups at the redshift of the primary cluster in the same *XMM* image are indicated in red, while blue points mark the remaining "isolated" galaxy groups. The dot-

Примеры площадок вокруг скоплений

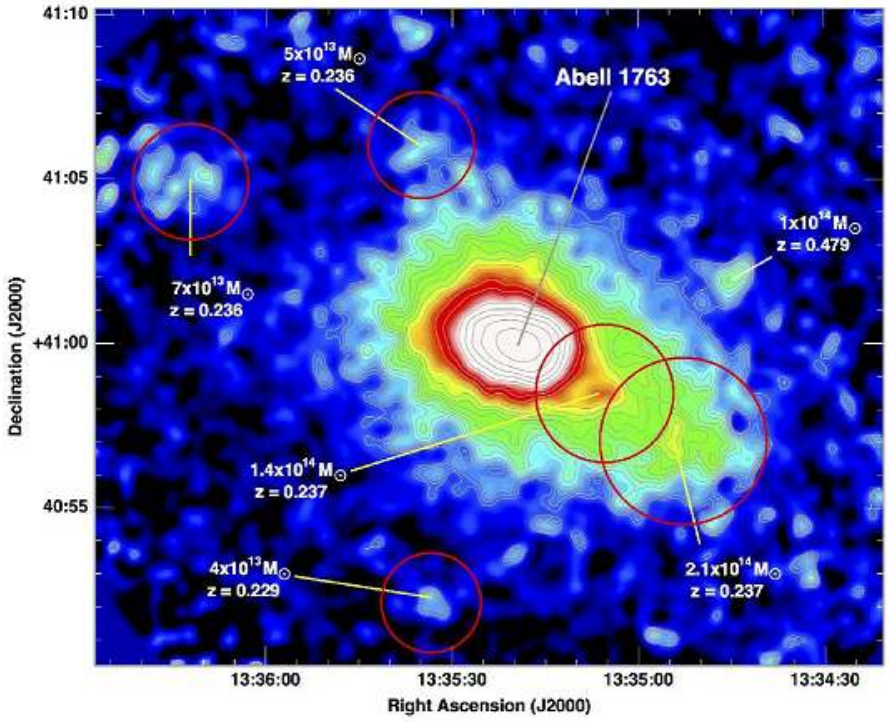

Figure 2. Extended X-ray emission from Abell 1763. All spectroscopically confirmed X-ray groups are indicated and labelled by their redshift and estimated M_{200} value. Those groups which are infalling into Abell 1763 are marked by red circles of diameter r_{200}.

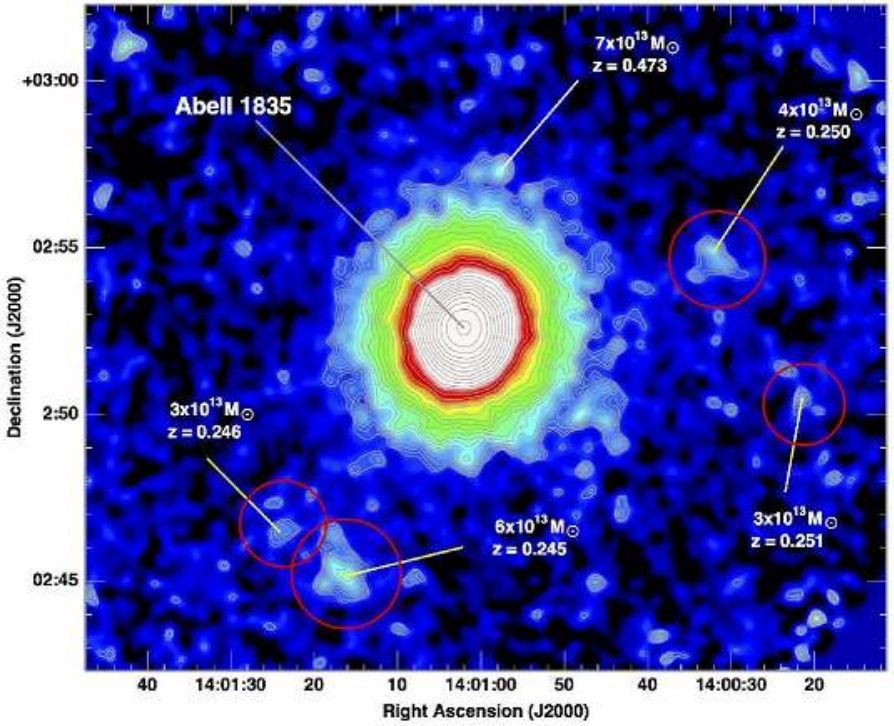

Figure 3. Extended X-ray emission from Abell 1835. All spectroscopically confirmed X-ray groups are indicated and labelled by their redshift and estimated M_{200} value. Those groups which are infalling into Abell 1835 are marked by red circles of diameter r_{200}.

Демонстрация динамической связи падающих групп и скоплений

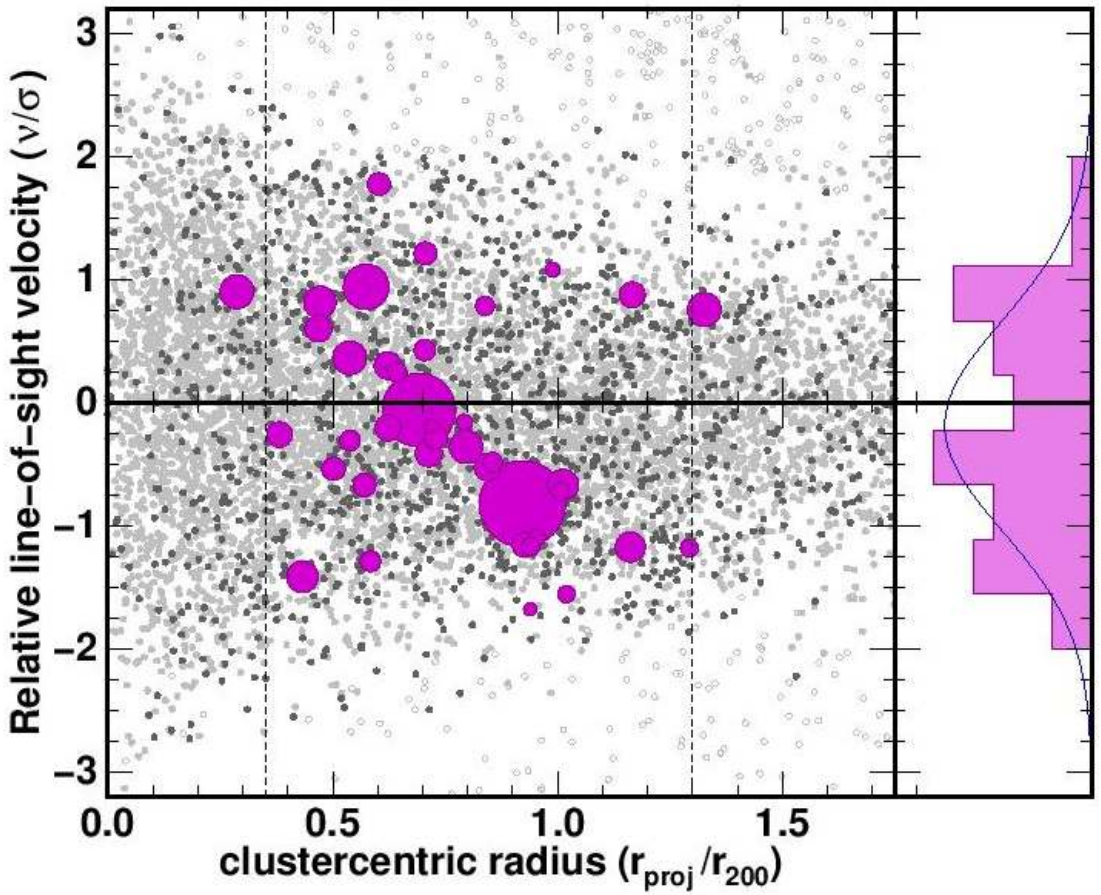

Figure 11. Stacked phase-space diagram, $(\nu_{los}-\langle\nu\rangle)/\sigma_\nu$ versus r_{proj}/r_{200} of the 39 XMM groups (*magenta symbols*) and member galaxies (*grey solid points*) for all 23 clusters in our sample. The size of each symbol indicates the group mass. Darker grey symbols indicating

А это модельный рост скоплений галактик в LCDM-симуляциях

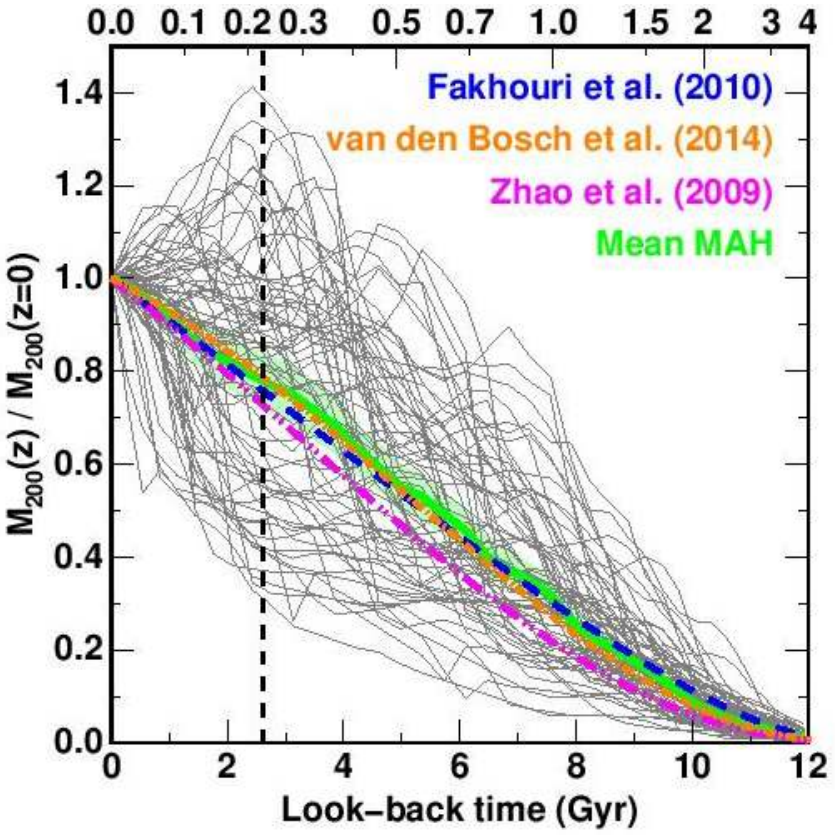

Figure 16. The mass accretion histories (MAHs) of the 75 most massive DM halos in the Millennium simulation (grey curves). The solid green curve indicates the mean MAH of these 75 halos, while the green shaded region indicates the expected 1σ range of MAHs when averaging over 23 clusters selected at random from

Последние выводы

- The average mass per cluster contained within these infalling X-ray groups is $2.2\times10^{14}\,M_{\odot}$, or $19\pm5\%$ of the mass of the primary cluster.
- We estimate that $\sim10^{15}\,M\odot$ clusters increase their masses by $16\pm4\%$ between $z=0.223$ and the present day due to the accretion of X-ray groups with $M_{200}\gtrsim10^{13.2}\,M_{\odot}$. This represents 35–50% of the expected mass growth of these clusters at these late epochs. The rest of the mass growth is likely to occur through the smooth accretion of dark matter not bound within DM halos.

Astro-ph: 1709.06963

DEEP CO(1-0) OBSERVATIONS OF $Z = 1.62$ CLUSTER GALAXIES WITH SUBSTANTIAL MOLECULAR GAS RESERVOIRS AND NORMAL STAR FORMATION EFFICIENCIES

Gregory Rudnick[1,2,3], Jacqueline Hodge[2,4,5,6], Fabian Walter[2], Ivelina Momcheva[7], Kim-Vy Tran[8], Casey Papovich[8], Elisabete da Cunha[2,10], Roberto Decarli[2], Amelie Saintonge[11], Christopher Willmer[9], Jennifer Lotz[12], Lindley Lentati[13]

ApJ in press

ABSTRACT

We present an extremely deep CO(1–0) observation of a confirmed $z = 1.62$ galaxy cluster. We detect two spectroscopically confirmed cluster members in CO(1–0) with $S/N > 5$. Both galaxies have $\log(\mathcal{M}_\star/\mathcal{M}_\odot) > 11$ and are gas rich, with $\mathcal{M}_{\rm mol}/(\mathcal{M}_\star+\mathcal{M}_{\rm mol}) \sim 0.17-0.45$. One of these galaxies lies on the star formation rate (SFR)-$\mathcal{M}_\star$ sequence while the other lies an order of magnitude below. We compare the cluster galaxies to other SFR-selected galaxies with CO measurements and find that they have CO luminosities consistent with expectations given their infrared luminosities. We also find that they have comparable gas fractions and star formation efficiencies (SFE) to what is expected from published field galaxy scaling relations. The galaxies are compact in their stellar light distribution, at the extreme end for all high redshift star-forming galaxies. However, their SFE is consistent with other field galaxies at comparable compactness. This is similar to two other sources selected in a blind CO survey of the HDF-N. Despite living in a highly quenched proto-cluster core, the molecular gas properties of these two galaxies, one of which may be in the processes of quenching, appear entirely consistent with field scaling relations between the molecular gas content, stellar mass, star formation rate, and redshift. We speculate that these cluster galaxies cannot have any further substantive gas accretion if they are to become members of the dominant passive population in $z < 1$ clusters.

Вот как выглядит это скопление на z=1.62

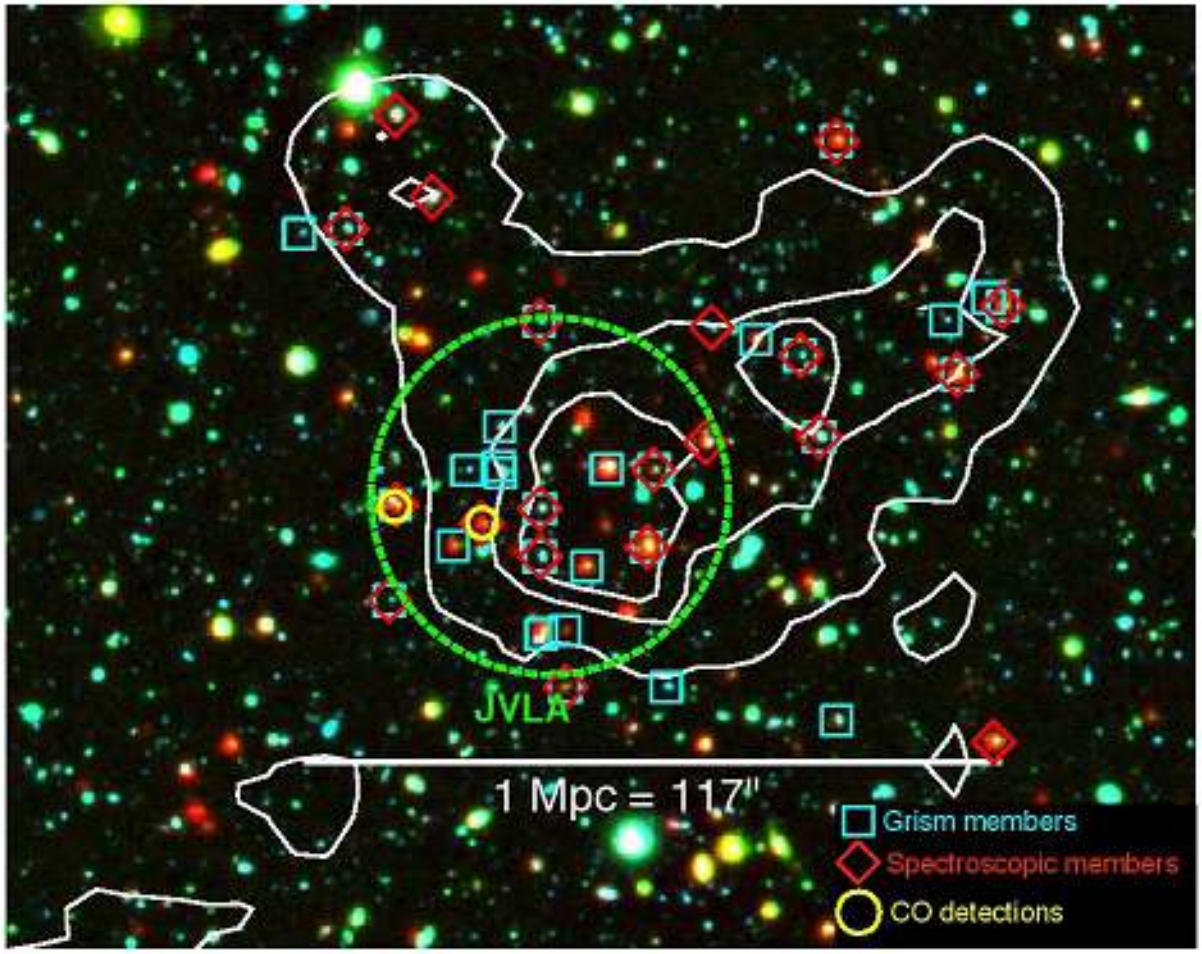

Figure 1. A $Bi[4.5\mu m]$ image of XMM-LSS J02182-05102. The contours denote regions with 5, 10, and 15σ above the mean density of galaxies with $1.5 < z_{phot} < 1.7$ from the UKIDSS UDS K-selected catalog presented in Papovich et al. (2010). The green dashed circle illustrates our pointing of the VLA, with the size of the circle corresponding to the FWHM of the beam at 43.913 GHz. The yellow circles indicate the two CO(1–0) detections. The red diamonds mark all spectroscopically confirmed members and the cyan squares mark all member as determined by their grism redshifts (Papovich et al. 2010; Tanaka et al. 2010; Tran et al. 2015, Momcheva et al. in prep.).

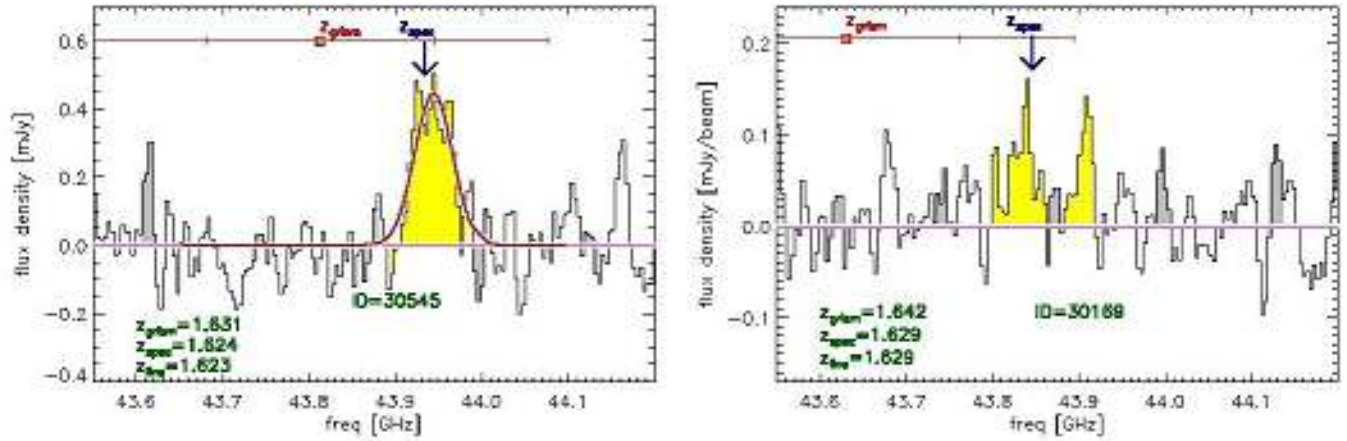

Figure 2. Two detections of CO(1–0) in star-forming cluster galaxies from our VLA data, shown at 4MHz resolution smoothed by 8MHz. The symbols at the top of each panel indicate the spectroscopic and HST/WFC3 grism redshift (Papovich et al. 2010; Tanaka et al. 2010; Tran et al. 2015, Momcheva et al. in prep.). The yellow regions correspond to the frequencies over which we collapsed the images to estimate the S/N and derive the contours shown in Figure 3. The gray portions of the spectra correspond to bad channels. For both sources we compute the line center using a Gaussian fit. For 30545 we show the Gaussian fit to the data but omit it from 30169 given the irregular velocity structure. The error bars on the grism redshifts are the 68 and 95% confidence intervals on the redshift.

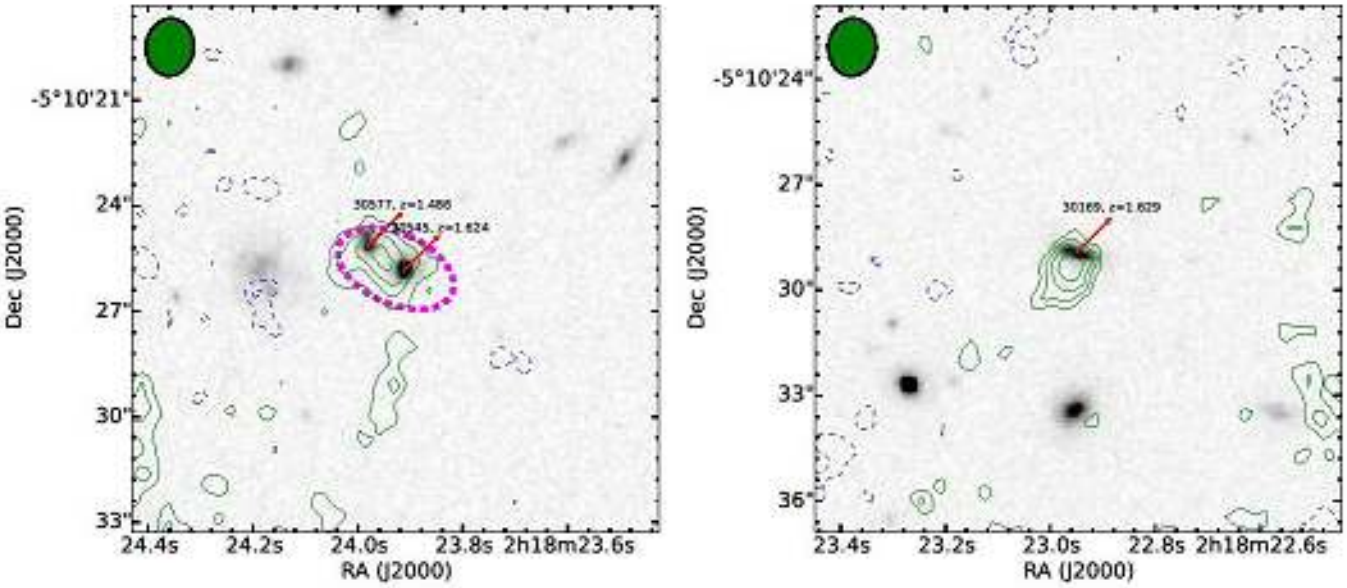

Обе галактики с заметным звездообразованием, но одна – ниже главной последовательности

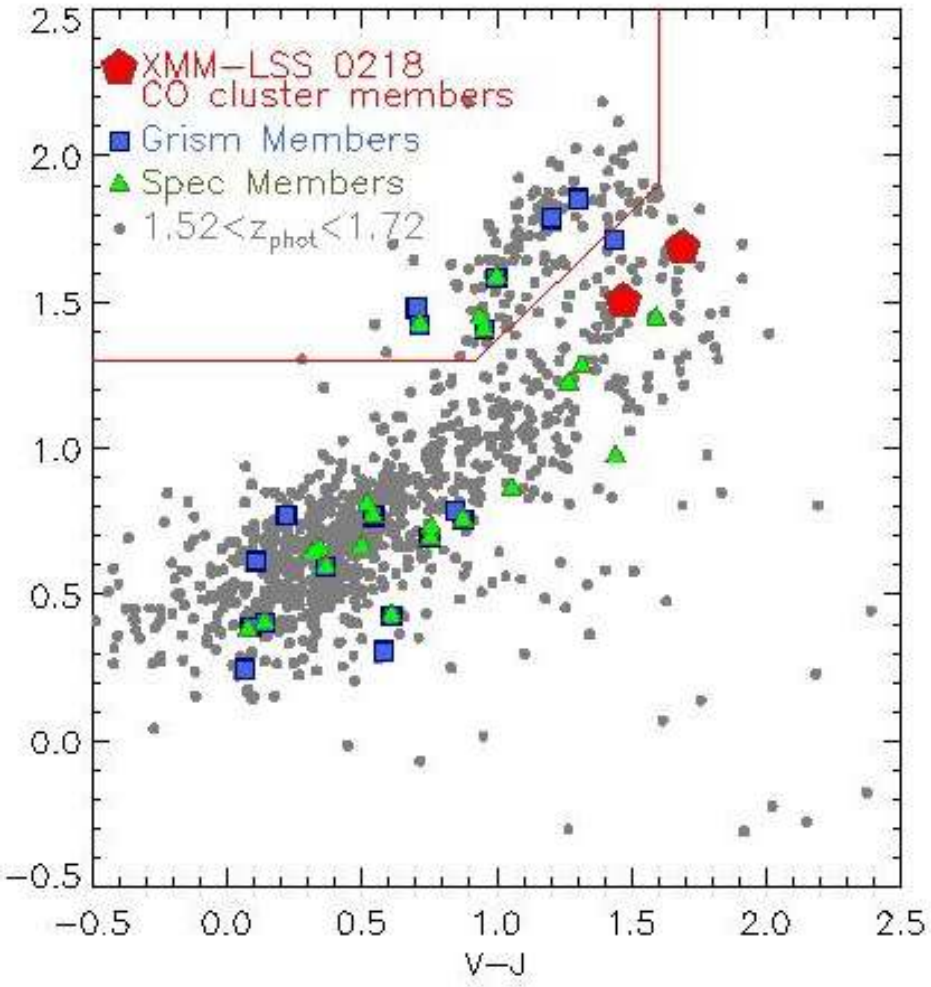

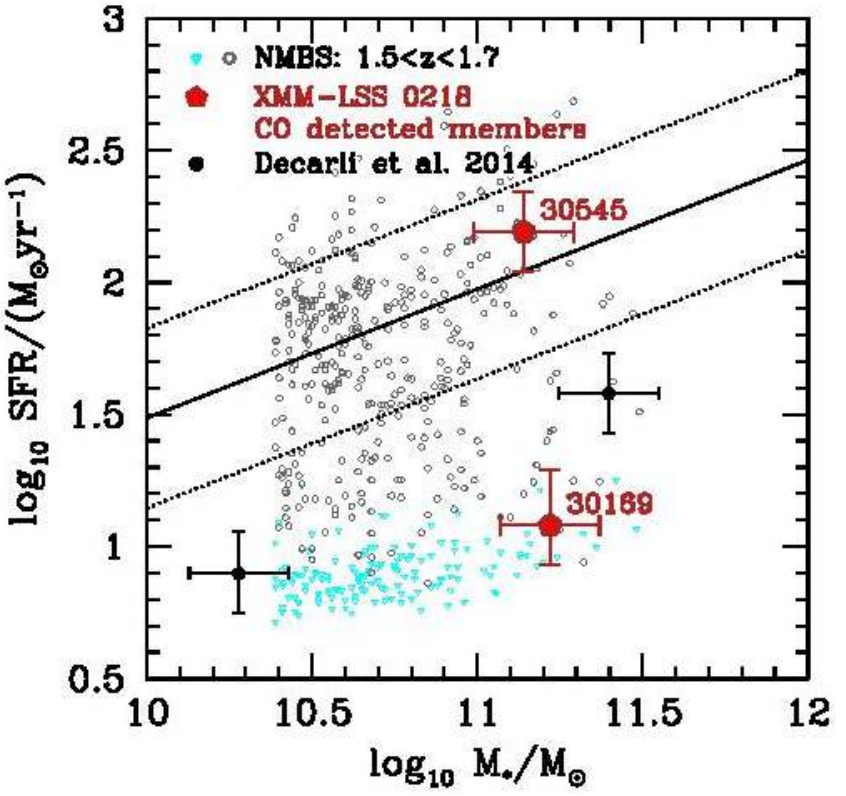

Figure 6. The $\mathcal{M}_\star$ and SFRs for our two sources compared to those from the NEWFIRM Medium Band Survey (NMBS; Whitaker et al. 2012). The SFRs from NMBS were computed using a combination of UV+IR. Galaxies with IR detections are shown as dark gray circles. Those not detected in the IR are indicated as 1σ upper limits with cyan triangles. The two CO detected sources

Результаты

Table 1
Stellar Population Parameters of CO-detected Galaxies

ID	$\log(\mathcal{M}_\star/\mathcal{M}_\odot)$[a]	SFR[a] $[\mathcal{M}_\odot\ \mathrm{yr}^{-1}]$	$\log(L_{IR}/L_\odot)$[a]	$r_{1/2}$[b] [kpc]	n[c]	q[d]
30169	$11.22^{+0.15}_{-0.15}$	$12.0^{+7.5}_{-3.5}$	$11.46^{+0.15}_{-0.15}$	4.15 ± 0.17	0.6 ± 0.1	0.23 ± 0.03
30545[e]	$11.14^{+0.15}_{-0.15}$	$155.6^{+64.2}_{-45.4}$	$12.23^{+0.15}_{-0.15}$	1.93 ± 0.15	2.7 ± 0.4	0.76 ± 0.05

[a] Computed from the MAGPHYS (da Cunha et al. 2008) fits to the full SED from the u-band through the *Herschel* SPIRE bands at 500μm. We assign a minimum 0.15 dex uncertainty to all quantities.
[b] The effective radius for a Sérsic (1968) fit to the F160W HST/WFC3 imaging from van der Wel et al. (2012).
[c] The Sérsic (1968) index of the fit to the F160W HST/WFC3 imaging from van der Wel et al. (2012).
[d] The minor-to-major axis ration of the fit to the F160W HST/WFC3 imaging from van der Wel et al. (2012).
[e] The observed optical and NIR photometry for this source are well separated from the neighbor 30577. It is possible that the MIPS 24μm and Herschel fluxes may include contributions from 30545 and the neighbor 30577. As the SFR is dominated by the FIR emission for the Herschel source, if it is blended we should still be measuring the total SFR corresponding to the CO detection.

Шкалирующие соотношения

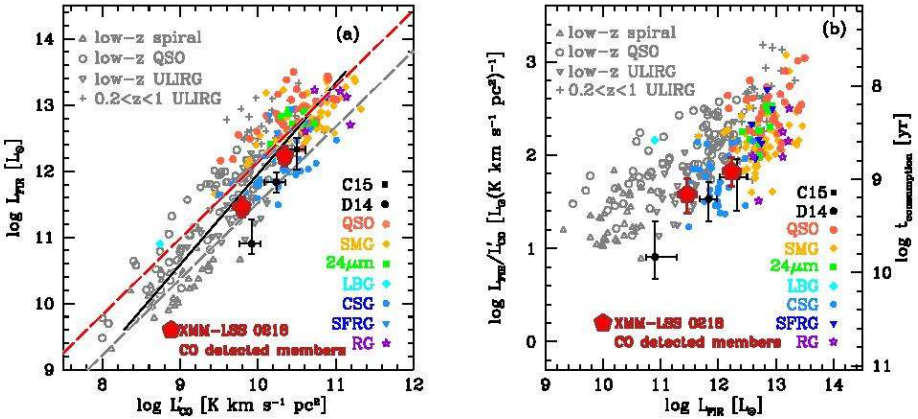

Figure 7. *Left Panel:* A comparison of the infrared luminosities and CO luminosities of our two CO detected cluster members at $z = 1.625$ (large filled Pentagons) with a sample of star-forming galaxies and QSOs over a wide range of redshift taken from Carilli & Walter (2013) and which includes various local galaxies as well as all systems detected in CO at $z > 1$ as of 2013. In addition, we show two galaxies from D14 that were detected in a blind CO survey of the HDF-N and one from Chapman et al. (2015, C15) that was detected in a blind survey of a proto-cluster at $z = 2.3$. L_{IR} is a proxy for the SFR and the L'_{CO} is a proxy for the gas mass, modulo α_{CO}. The solid line is a fit to all data points, which gives a slope of 1.35 ± 0.04. The dashed lines indicate the best fits for the main sequence galaxies (gray) and starburst galaxies (red) derived by Genzel et al. (2010) and Daddi et al. (2010a). *Right Panel:* We compare the ratio of L_{IR}/L'_{CO} to L_{IR} for the same galaxies as shown in the left-hand panel. L_{IR}/L'_{CO} is a proxy for SFR/$\mathcal{M}_{\rm mol}$ or the star formation efficiency. On the right axis we plot the consumption timescale. Our two cluster members are forming stars with typical SFE and have $t_{\rm con}$ similar to other gas-rich galaxies at their L_{IR}. The legend abbreviations in both plots stand for: QSO – quasi-stellar objects; SMG – submillimeter

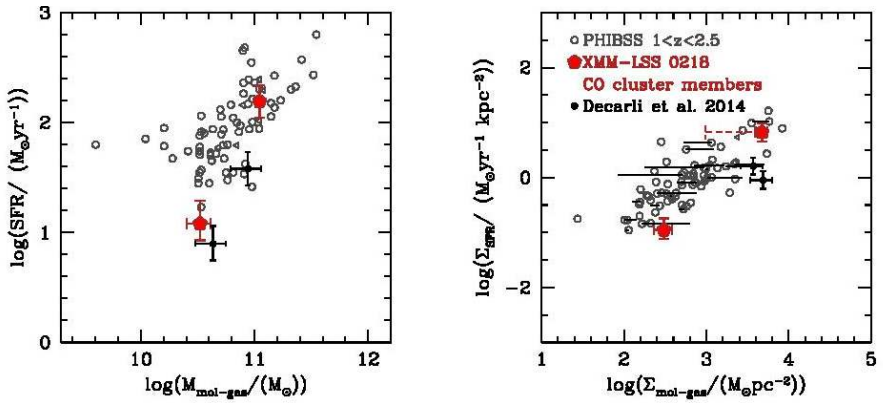

Figure 9. *Left Panel:* The SFR and molecular gas mass for our two CO detected cluster members, galaxies from PHIBSS (Tacconi et al. 2013) and the two blind detections from Decarli et al. (2014). We convert L'_{CO} to gas mass using a Milky Way α_{CO}. 30169 has a SFR lower than the PHIBSS sources while 30545 is consistent with the distribution of PHIBSS sources in $\mathcal{M}_{\rm mol}$ and SFR. *Right Panel:* The surface density of star formation and molecular gas for the same sources. In this diagram the star formation efficiency decreases down and to the right. 30169 has a Σ_{SFR} less than nearly all of the PHIBSS points while 30545 is at the upper end of the distribution and is consistent with the PHIBSS distribution. The dashed error bar on the upper red point (30545) shows how the SFR surface density would change if integrated over the extend of the resolved CO line instead of over the stellar disk. If this is appropriate then the SFE for 30545 would be higher than that of galaxies in the PHIBSS sample. A more precise comparison will require actual gas size measurements for our sources. Note that the same size is used for both the SFR and gas surface density for all measurements and this may partly explain the strong correlation between the two parameters in the right-hand panel. The horizontal black lines on the Tacconi et al. (2013) points show

Отличие галактик в скоплениях: время исчерпания газа(?) и поверхностная плотность звезд

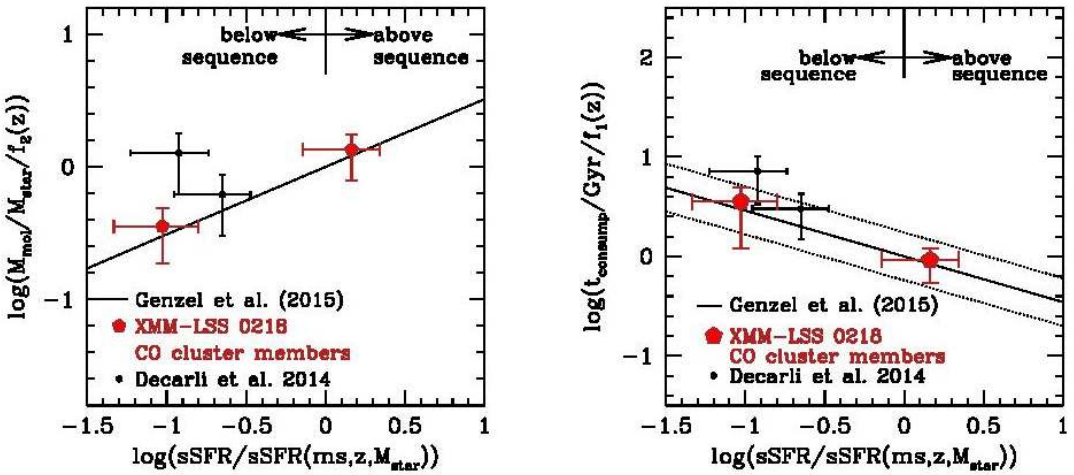

Figure 10. A comparison of our galaxies with the scaling relations from Genzel et al. (2015). In both panels, the x-axis is the distance from the main sequence, which is parameterized, as in Genzel et al. (2015), using the relation from Whitaker et al. (2012). Both scaling relations and galaxies have had the stellar mass and redshift dependence removed (see text.) *Left Panel:* The molecular gas fraction of our galaxies and those of Decarli et al. (2014). The four galaxies have gas fractions consistent with the scaling relations. *Right panel:* The consumption timescales for the same four galaxies. The dotted lines indicate the 0.24 dex scatter around the scaling relation from Genzel et al. (2015). All four galaxies have $t_{\rm con}$ consistent with the scaling relations.

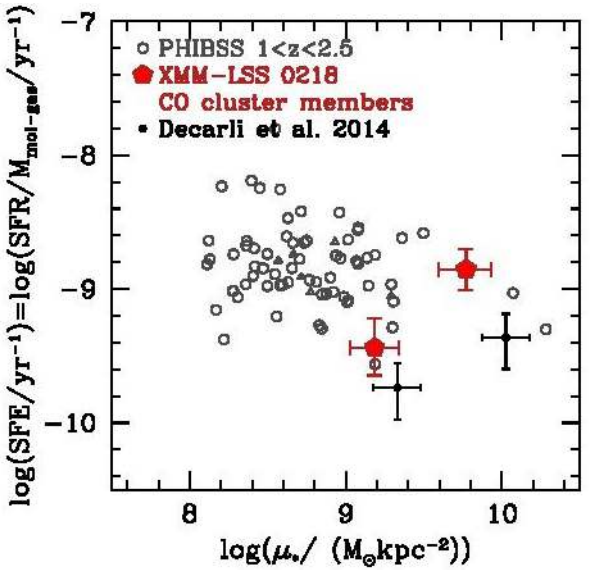

Figure 11. The Star Formation Efficiency (SFE≡SFR/$\mathcal{M}_{\rm mol}$) vs the stellar surface mass density for our two CO detected cluster members, galaxies from PHIBSS (Tacconi et al. 2013) and the two blind detections from Decarli et al. (2014). We convert L'_{CO} to gas mass using a Milky Way $\alpha_{\rm CO}$, which is consistent with the dynamical constraints from the CO line width and the rest-frame optical size. Our galaxies and the two other blind detections are at the extreme high end of surface mass density.

Astro-ph: 1709.07003

LOW METALLICITIES AND OLD AGES FOR THREE ULTRA-DIFFUSE GALAXIES IN THE COMA CLUSTER

MENG GU[1], CHARLIE CONROY[1], DAVID LAW[2], PIETER VAN DOKKUM[3], RENBIN YAN[4], DAVID WAKE[5], KEVIN BUNDY[6], ALLISON MERRITT[3], ROBERTO ABRAHAM[7], JIELAI ZHANG[7,8,9], MATTHEW BERSHADY[10], DMITRY BIZYAEV[11,12], JONATHAN BRINKMANN[11], NIV DRORY[13], KATHLEEN GRABOWSKI[11], KAREN MASTERS[14], KAIKE PAN[11], JOHN PAREJKO[15], ANNE-MARIE WEIJMANS[16], KAI ZHANG[17]

submitted to The Astrophysical Journal.

ABSTRACT

A large population of ultra-diffuse galaxies (UDGs) was recently discovered in the Coma cluster. Here we present optical spectra of three such UDGs, DF 7, DF 44 and DF 17, which have central surface brightnesses of $\mu_g \approx 24.4-25.1$ mag arcsec^{-2}. The spectra were acquired as part of an ancillary program within the SDSS-IV MaNGA Survey. We stacked 19 fibers in the central regions from larger integral field units (IFUs) per source. With over 13.5 hours of on-source integration we achieved a mean signal-to-noise ratio (S/N) in the optical of 9.5Å^{-1}, 7.9Å^{-1} and 5.0Å^{-1}, respectively, for DF 7, DF 44 and DF 17. Stellar population models applied to these spectra enable measurements of recession velocities, ages and metallicities. The recession velocities of DF 7, DF 44 and DF 17 are 6599^{+40}_{-25} km/s, 6402^{+41}_{-39} km/s and 8315^{+43}_{-43} km/s, spectroscopically confirming that all of them reside in the Coma cluster. The stellar populations of these three galaxies are old and metal-poor, with ages of $7.9^{+3.6}_{-2.5}$ Gyr, $8.9^{+4.3}_{-3.3}$ Gyr and $9.1^{+3.9}_{-5.5}$ Gyr, and iron abundances of [Fe/H] $-1.0^{+0.3}_{-0.4}$, $-1.3^{+0.4}_{-0.4}$ and $-0.8^{+0.5}_{-0.5}$, respectively. Their stellar masses are $3-6\times10^8 M_\odot$. The UDGs in our sample are as old or older than galaxies at similar stellar mass or velocity dispersion (only DF 44 has an independently measured dispersion). They all follow the well-established stellar mass—stellar metallicity relation, while DF 44 lies below the velocity dispersion-metallicity relation. These results, combined with the fact that UDGs are unusually large for their stellar mass, suggest that stellar mass plays a more important role in setting stellar population properties for these galaxies than either size or surface brightness.

Фиберы MANGa на трех UDG Coma

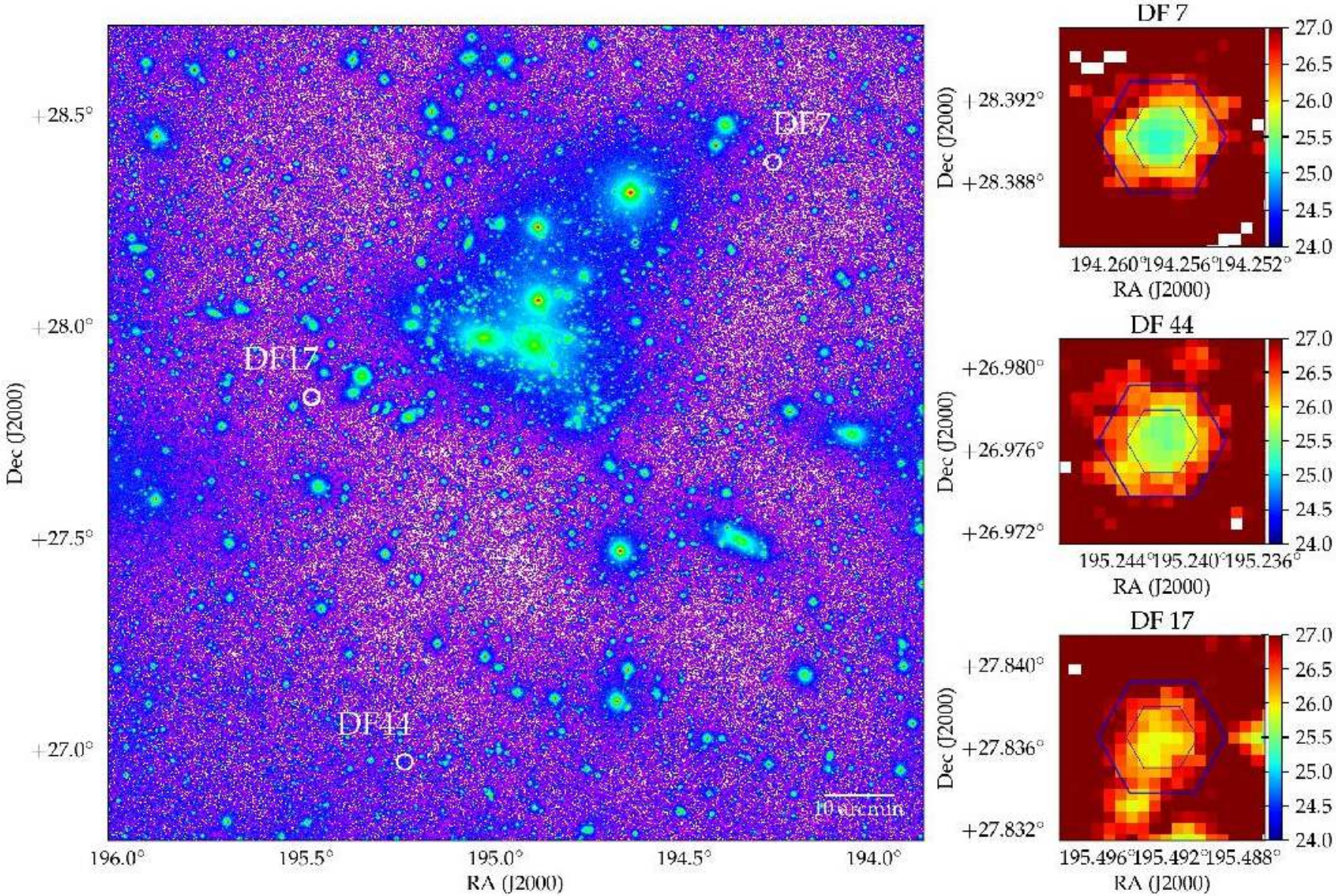

Пример интегрального спектра

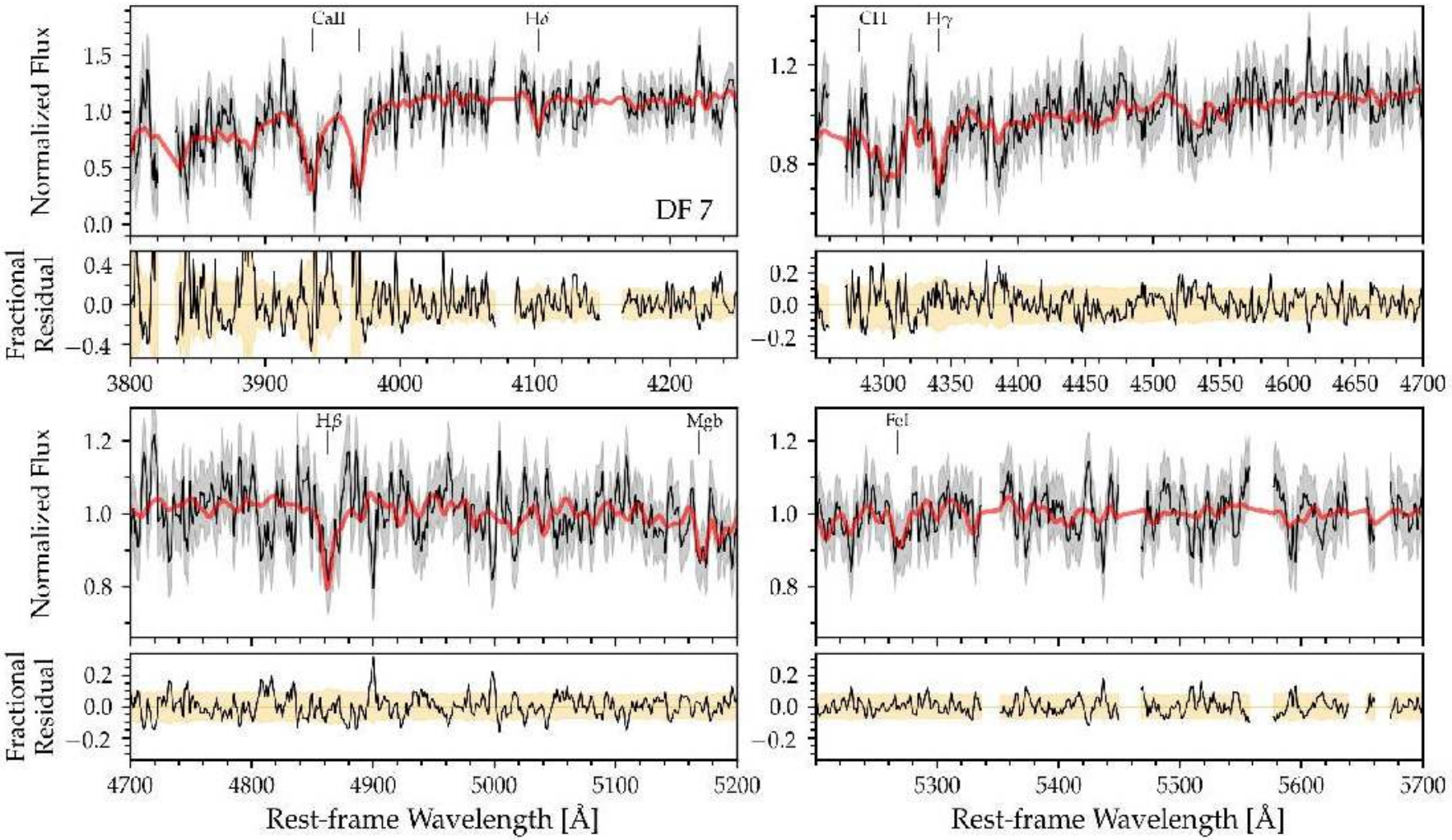

Результаты по звездному населению

Target	DF 7	DF 44	DF 17
α	$12^h57^m01.7^s$	13h00m58.0s	13h01m58.3s
δ	$28°23'25''$	$26°58'35''$	$27°50'11''$
$\mu_{0,g}$ (mag/arcsec^{-2})	24.4 ± 0.5	24.5 ± 0.5	25.1 ± 0.5
M_g (mag)	$-16.0^{+0.2}_{-0.2}$	$-15.7^{+0.2}_{-0.2}$	$-15.2^{+0.3}_{-0.2}$
R_{eff} (kpc)	$4.3^{+1.4}_{-0.8}$	$4.6^{+1.5}_{-0.8}$	$4.4^{+1.5}_{-0.9}$
S/N (4500−5000Å)	9.5Å^{-1}	7.9Å^{-1}	5.0Å^{-1}
Constraints from Spectra			
Velocity (km/s)	6600^{+40}_{-26}	6402^{+41}_{-38}	8311^{+43}_{-43}
log(age/Gyr)	$0.93^{+0.17}_{-0.18}$	$1.02^{+0.11}_{-0.24}$	$0.88^{+0.22}_{-0.42}$
[Fe/H]	$-1.03^{+0.31}_{-0.34}$	$-1.25^{+0.33}_{-0.39}$	$-0.83^{+0.56}_{-0.51}$
$(M/L)_r$	$1.63^{+0.55}_{-0.29}$	$1.86^{+0.39}_{-0.56}$	$1.54^{+0.71}_{-0.52}$
$\log(M_\star/M_\odot)$	$8.74^{+0.17}_{-0.11}$	$8.66^{+0.12}_{-0.15}$	$8.42^{+0.22}_{-0.19}$
Combined Constraints from Spectra and Photometry			
Velocity (km/s)	6599^{+40}_{-25}	6402^{+41}_{-39}	8315^{+43}_{-43}
log(age/Gyr)	$0.90^{+0.17}_{-0.16}$	$0.95^{+0.17}_{-0.20}$	$0.96^{+0.16}_{-0.40}$
[Fe/H]	$-1.04^{+0.32}_{-0.36}$	$-1.25^{+0.35}_{-0.41}$	$-0.80^{+0.49}_{-0.47}$
$(M/L)_r$	$1.56^{+0.47}_{-0.28}$	$1.64^{+0.54}_{-0.38}$	$1.80^{+0.51}_{-0.66}$
$\log(M_\star/M_\odot)$	$8.72^{+0.17}_{-0.13}$	$8.61^{+0.16}_{-0.11}$	$8.49^{+0.15}_{-0.20}$

Нетипичен именно возраст звезд